ELSEVIER

Journal of Nuclear Materials 253 (1998) 104–112

journal of nuclear materials

Damage calculation in fusion ceramics: comparing neutrons and light ions

P.V. Vladimirov [a], D. Lizunov [a], Yu.A.I. Ryazanov [a], A. Möslang [b,*]

[a] *RRC 'Kurchatov Institute', 123182 Moscow, Russia*

[b] *Institut fur Materialforschung, Forschungszentrum Karlsruhe, Postfach 3640, 76021 Karlsruhe, Germany*

Abstract

A method developed earlier for displacement damage calculations in compound materials is applied to fusion ceramics irradiated by various neutron sources and light ion accelerators. For protons up to 40 MeV and alpha-particles up to 100 MeV, as well as for several neutron environments (EEF, ITER, HFIR, FFTF), sublattice-specific primary recoil spectra and displacement damage rates have been calculated for α-Al_2O_3, AlN, BeO, MgO, $MgAl_2O_4$ and SiC. Although the primary recoil spectra can vary significantly for different neutron sources and light ions, the ratios of sublattice-specific damage rates are the same within 5% for BeO, MgO and SiC in all considered environments. For ceramics containing Al, the damage ratio differs up to about 40% between neutron and light ion irradiations. © 1998 Elsevier Science B.V.

1. Introduction

A broad spectrum of radiation-induced property changes of various ceramics has been reported and reviewed [1–3], reflecting their growing importance for the engineering design of ITER and other fusion reactor devices. For ceramics like α-Al_2O_3 or $MgAl_2O_4$, irradiation-induced microstructural changes, swelling and, more recently, electrical properties have already been investigated with different irradiation sources up to higher displacement damage levels. A significant fraction of the irradiation sources used for ceramics irradiations is based on 2–20 MeV protons [4–9], 28–104 MeV alpha-particles [10–12], ≤ 4 MeV heavy ions [13], fission neutrons [14–16] and 14 MeV neutrons [17,18].

For all these bombarding particles the damage calculations involve calculating the primary knocked-on atom (PKA) spectra, which is a separate elaborate task for the neutron irradiation [23]. With some exceptions [19,38,40], the PKA-induced displacement damage calculations in polyatomic materials are still based on an analytical approach for quasi-monoatomic materials originally proposed by Lindhard et al. [20,21]. This approach has been developed further by Torrens et al. [22]. However, such an approach to materials with significant differences in atomic masses and/or displacement threshold energy E_d values can lead to differences of as much as 50% with respect to the total displacement damage as shown by Greenwood [23]. That is why the bulk of the data currently available on irradiated ceramics represents only a first-step approximation to the real displacement damage level.

In this paper we will discuss the application of an earlier-proposed method for displacement damage calculation in compound materials and ceramic materials. The problem is treated in terms of linear Boltzmann transport equation. In the case of neutron irradiation the whole problem is divided in two parts. First, the PKA spectrum is calculated by means of the NJOY code. The second step implements the calculation of the PKA transport and the associated radiation damage by the BOLT code [25,26]. In our previous work, this method was applied to several high-temperature superconducting ceramics [24]. It was shown that the proposed method is especially suitable for displacement damage calculations in compound materials with significantly different atomic masses and/or E_d-values. The development of fusion ceramics is closely related to the simulation of fusion conditions by means of ion accelerators and fission neutrons. Therefore, detailed knowledge of the PKA spectra and the displacement dam-

* Corresponding author. Fax: +49-7247 824 567; e-mail: anton.moeslang@imf.fzk.de.

PII S0022-3115(97)00339-5

age rates is needed for both types of experiments. The proposed method allows us to calculate damage rates for both ion and neutron irradiations within the same physical model and the same numerical approach. It provides therefore a reliable tool for calculating damage rates in ceramics as well as for directly comparing different types of irradiation sources. Besides calculating the total number of displaced atoms, it calculates the number of displaced atoms of each constituent separately.

2. Recoil transport calculations

Most of the features of the algorithm used by the BOLT program were described in details earlier [25–27]. The code solves a time-independent system of linear Boltzmann transport equations for slowing down ions and knocked-on atoms in one-dimensional, planar geometry. We define the x-axis as directed perpendicular to the target surface along with the incident beam. The slowing down of particles is described in the program by two independent processes: (i) continuous slowing down of ions due to interaction with the electron subsystem, as described by the electronic stopping power $S_k(E)$ and (ii) discrete binary elastic collisions with target atoms. Introducing the scalar flux $\Phi_k(x, \Omega, E)$ for the kth sort of moving atoms that can be either knocked-on atoms or slowing down ions, we can write

$$(\Omega * e_x)\frac{\mathrm{d}\Phi_k(x, \Omega, E)}{\mathrm{d}x} - \frac{\mathrm{d}}{\mathrm{d}E}\left[S_k(E)\Phi_k(x, \Omega, E)\right] = I_k + q_k(x, \Omega, E), \quad (1)$$

where $S_k(E)$ is the electronic stopping power for the kth sort of moving atoms, e_x is the unit vector along the x-axis and $q_k(x, \Omega, E)$ is the source of the k-type of moving atoms. I_k stands for the collision integral of the kth sort of moving particles:

$$I_k = \sum_i N_i \int \mathrm{d}\sigma_{ki}(E', \Omega' \to E, \Omega; \Omega'')\Phi_k(x, \Omega', E')\,\mathrm{d}E'\,\mathrm{d}\Omega' - \sum_i N_i \Phi_k(x, \Omega, E)\int \mathrm{d}\sigma_{ki}(E, \Omega \to E', \Omega'; \Omega'')\,\mathrm{d}E'\,\mathrm{d}\Omega' + N_k \sum_i \int \mathrm{d}\sigma_{ik}(E', \Omega' \to E' - E, \Omega''; \Omega)\Phi_i(x, \Omega', E')\,\mathrm{d}E'\,\mathrm{d}\Omega', \quad (2)$$

where N_i is the atomic concentration of the ith sort of atoms and $\mathrm{d}\sigma_{ki}(E, \Omega \to E', \Omega'; \Omega'')$ is a differential cross-section of collisions between the kth type of atoms, with energy E moving in Ω direction and the ith type of atoms in the target. Eq. (2) is solved numerically by a multi-group method from high energies down to low energies. The main feature of the BOLT code is that it treats all the types of moving atoms in the same manner. Bombarding ions are treated like target atoms with zero concentration in the target. Such an approach allows us to calculate the kinematics of collisions between atoms of different masses in an accurate manner. For the damage calculations we use a threshold displacement model [28]. The code allows us to correctly treat different threshold energies E_d for various components of the target. We do it by setting the lower limit of the integral in the third term of Eq. (2), describing the generation of new knocked-on atoms to the specific E_d^k value of the kth component. The total displacement functions used here are similar to those originally described by Parkin and Coulter [19]. However, in contrast to these earlier approaches, the BOLT code describes the continuous slowing down of the projectiles from high energies to low energies (and not vice versa); thus, it automatically circumvents certain difficulties in setting proper initial conditions for integral equations involved. It makes the code highly suitable for radiation damage calculations in multicomponent ceramics. The energy range and limiting values in the other integrals in Eq. (2) are defined as follows:

$$E_0 \geq E \geq \min_k\left(E_\mathrm{d}^k\right) = E_{\min},$$

where E_0 stands for the source energy. Thus, collisions with energy transfer of less than E_d produce some additional energy loss but no knocked-on atoms or displacement damage. The program calculates damage distributions for particular target components. These are assumed to be the third term in Eq. (2) integrated by E and Ω.

$$D_k(x) = N_k \int \mathrm{d}E\,\mathrm{d}\Omega \sum_i \int \mathrm{d}\sigma_{ik}(E', \Omega' \to E' - E, \Omega''; \Omega)\Phi_i(x, \Omega', E')\,\mathrm{d}E'\,\mathrm{d}\Omega'. \quad (3)$$

The physical parameters necessary for the solution of Eq. (1) are $S_k(E)$ and a differential cross-section for interatomic collisions. The algorithm for the solution of Eq. (1) was described in detail previously for a more general case of ion irradiation [26].

3. Neutron damage calculation

Radiation damage calculations under neutron irradiation include determining the primary recoil spectrum (PRS) of target atoms. The PRS depends on the neutron scattering cross-sections for target components and the neutron environment. The i-type PKA generation rate is defined as follows:

$$q_i(T) = \int \mathrm{d}E_n F(E_n) \sum_r N_i \frac{\mathrm{d}\sigma_i^r(E_n, T)}{\mathrm{d}T}, \quad (4)$$

where $F(E_n)$ is the energy spectrum of neutrons, $\mathrm{d}\sigma_i(E_n, T)/\mathrm{d}T$ is the differential cross-section of energy transfer T to the i-type recoil by neutron with energy E_n in the

particular nuclear channel r. We use these spectra as a source term in Eq. (1) for the displacement damage calculations.

Neutron cross-sections for different kinds of nuclei as well as energy and angular distributions of scattered neutrons are available in different evaluated nuclear data files. In the present work we have used the ENDF-VI library in ENDF/B-6 format [29]. The NJOY code [30] was used for multi-group PKA spectra calculations. Only elastic and discrete inelastic reactions were considered. For these nuclear channels the recoil atom energy is fully determined by energy and momentum conservation laws.

Neutrons that are able to produce significant damage have mean free paths several orders of magnitude greater than that those of PKAs. So in the case of neutron irradiation the space-independent form of the Boltzmann transport equation is used. Damage rates for particular sublattices of the target in this case can also be obtained as shown in Eq. (3) with the space variable x omitted.

The rate of k-type atomic displacements D_k can be expressed in terms of the partial damage cross-sections $\sigma_{\mathrm{d}}^{k}(E_n)$:

$$D_k = N_k \int \mathrm{d}E_n \sigma_{\mathrm{d}}^{k}(E_n) F(E_n). \tag{5}$$

Introducing the partial spectral-averaged damage cross-section $\overline{\sigma_{\mathrm{d}}^{k}}$ [31]:

$$\overline{\sigma_{\mathrm{d}}^{k}} = \frac{\int \mathrm{d}E_n \sigma_{\mathrm{d}}^{k}(E_n) F(E_n)}{\int \mathrm{d}E_n F(E_n)} = \frac{D_k}{N_k F_{\mathrm{tot}}}, \tag{6}$$

we obtain an expression able to compare different types of irradiation sources. Here $F_{\mathrm{tot}} = \int \mathrm{d}E_n F(E_n)$ is the total neutron flux. The damage rates D_k for particular target components were obtained directly from the Boltzmann equation solution.

The displacement damage cross-sections defined by Eq. (6) are independent of the atomic density, while the radiation damage rates are proportional to the atomic concentration of species in the material. To omit this concentration dependence one should express results in displacements per atom (DPA) units, which is straightforward in the case of monoatomic targets. We shall discuss the usage of this notion for ceramic materials later.

4. Results and discussion

4.1. Neutron group and PKA spectra

Radiation damage calculations have been performed for two prospective fusion facilities and for two fission reactors which are widely used for the simulation of fusion irradiation conditions. The set of neutron spectra used in the calculations is presented in Fig. 1. The fast flux test facility (FFTF) spectrum represents a fast neutron spectrum, while the high flux isotope reactor (HFIR) spectrum is a typical example of a mixed-spectrum reactor. EEF-FW and ITER1 are the spectra of the first-wall position in Tokamak-type fusion reactor concepts [32–34]. While the ITER1-spectrum has a flat shape except for a 14-MeV

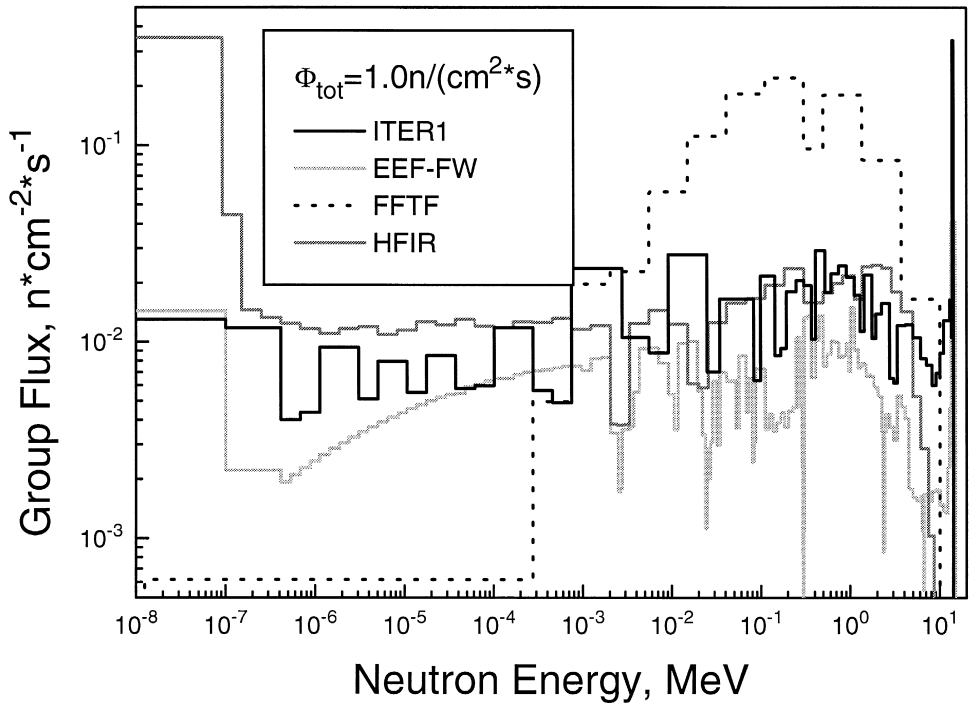

Fig. 1. Neutron group spectra for fusion environments (EEF, ITER) and for widely used fission reactors (HFIR, FFTF).

Table 1
Description of positions in ITER used for calculations

Position	Description of neutron spectrum	Total flux, n/(m^2 s)
ITER 1	first-wall point #1 in the first-wall Be zone	$2.97 \cdot 10^{18}$
ITER 2	back-plate point #2 in the outer-blanket center	$2.80 \cdot 10^{17}$
ITER 3	vessel-front-wall center point #3	$2.86 \cdot 10^{17}$
ITER 4	vessel-rear-wall center point #4	$1.44 \cdot 10^{16}$
ITER 5	TFC insulator center point #5	$5.28 \cdot 10^{15}$
ITER 6	central-port-case point #6 on the boundary with central-port-void	$5.69 \cdot 10^{17}$

peak, the FFTF reactor shows a pronounced maximum between about 0.03 and 3 MeV. Except for the missing high-energy tail and the relatively high density of thermal neutrons, the mixed-neutron spectrum of HFIR represents an energy range between 5×10^{-6} MeV and a few MeV; this is a reasonable approximation to a typical spectrum in a plasma-facing position for ITER. For six different positions in ITER, Table 1 shows the total neutron flux ranging over more than three decades from 2.97×10^{18} to 5.28×10^{15} n/(m^2 s), that is, from very high to low flux regimes. In general, for ceramic insulator applications the neutron spectral energies will vary from nearly pure 14-MeV neutrons for plasma diagnostics to highly shielded areas with neutron spectra similar to those of thermal neutrons.

The primary recoil spectra were calculated for the most relevant isotopes of the ceramics BeO, MgO, Al_2O_3, $MgAl_2O_4$, SiC and AlN considered in this work. Some examples of PRS are given in Figs. 2 and 3 for the relevant isotopes $^{27}_{13}$Al and $^{16}_{8}$O irradiated under several neutron irradiation conditions. It is important to note that the high-energy tail of plasma-facing-fusion neutrons leads to pronounced peaks in the Al and O recoil spectra at 0.7 and 1.3 MeV, respectively; these PKA species cannot be matched at all by the spectra of fission neutrons. On the other hand, these peaks largely disappear when going from a first-wall position (ITER1) to the vessel-rear-wall position (ITER4), indicating that the latter can already be simulated fairly well by the mixed-spectrum reactor HFIR.

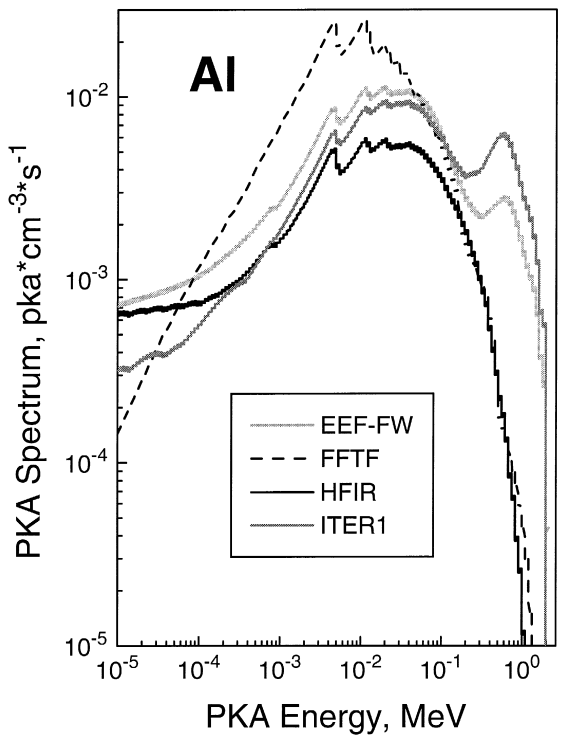

Fig. 2. Primary recoil aluminum spectra for several neutron environments. All neutron fluxes are normalized to the total flux of 10^{18} n/(m^2 s).

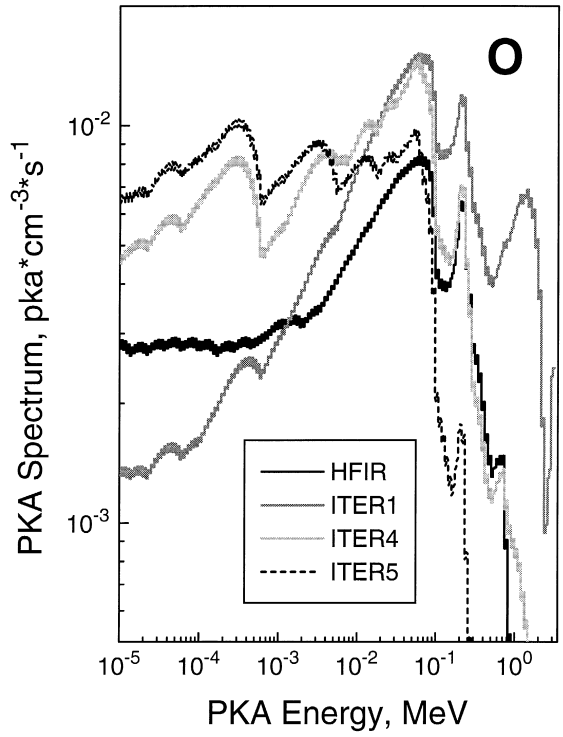

Fig. 3. Primary recoil oxygen spectra for several neutron environments. All neutron fluxes are normalized to the total flux of 10^{18} n/(m^2 s).

The recoil spectra of the other isotopes investigated show similar differences between fission and fusion neutrons, although their shape varies from isotope to isotope.

The development of radiation-resistant materials for fusion reactors relies on the correlation of test data obtained in a variety of neutron spectra, none of which are similar to those in the plasma-facing positions of Tokamak fusion reactors. While in metals the recoil energy spectra have very often shown themselves to be a major parameter that controls the defect morphology, and, thus, the macroscopic materials behavior, in most of the proposed ceramics similar studies have yet to be performed. Agnew [35] has irradiated sapphire with a variety of ion beams ranging from 50 keV hydrogen to 400 keV krypton and investigated the efficiency of point defect production by monitoring the oxygen vacancy color-center density without finding 'cascade effects' [3]. Although this result should not be generalized or transferred to neutron and high-energy light ion sources (because of differences in ion ranges, DPA, and energy deposition rates) these results suggest that, to a first approximation, differences in PRS may not produce different defect states in Al_2O_3. An analogous behavior was found by Zinkle [36], who compared Al with Al_2O_3 by plotting the surviving defect fraction versus the average PKA energy. These results suggest that (i) Al has a factor of 2 to 3 more surviving point defects and (ii) the surviving defect fraction in Al_2O_3 is within the scatter band of the published data that, in contrast to aluminum, is practically independent of the average PKA energy. The Al data were obtained below 10 K, where interstitials are certainly immobile. A straightforward explanation of the observed discrepancy in the surviving defect fraction could be that, during the Al_2O_3 irradiation experiments, the temperature of 80 K was already too high to suppress long-range diffusion and recombination of point defects. However, if a rigorous analysis of the existing database, together with well-defined future experiments, confirmed the above results on surviving point defects and their insensitivity to PKA spectra, practically all codes able to calculate the dpa rates in ceramics would need to be adapted with respect to the displacement damage efficiency.

4.2. Displacement damage rates

As a result of transport calculations, besides the distribution of particles in the phase space, we obtain the damage profiles as well as the total numbers of displaced atoms for each type of target atom. For practical applications, one should express the damage parameters in terms of relative damage of the particular sublattice for certain irradiation environments. In the case of monoatomic targets this leads to the well known notion of the radiation damage in displacements-per-atom (DPA) units. For multicomponent targets the extension of the DPA notion is not straightforward because the relative damage rates are different for individual sublattices of the target. Although for some polyatomic materials relevant aspects of irradiation damage (such as the PKA-energy dependence of the displacement efficiency [37,38] or the influence of different stopping powers on damage rates [39]) have already been developed in detail, sublattice-specific DPA rates for relevant irradiation sources are generally not available. In principle, the displacement damage density D_k of each constituent k as calculated by the BOLT code can be either normalized to the related atomic density N_k of that constituent, or it can be normalized to the total density $\sum N_k$ of the polyatomic target. Consider a two-component target with the densities of the components N_1 and N_2 and the displaced atom generation rates D_1 and D_2 per unit

Table 2
Partial contributions to displacement damage rate (10^{-7} dpa/s) in ceramics for several neutron facilities. All neutron fluxes are normalized to the total flux of 10^{18} n/(m^2 s) and the light ions to a beam current of 10^{-2} A/m^2

Material	Elem.	E_d (eV)	EEF	FFTF	HFIR	ITER1	He 104 MeV	H 18 MeV
BeO	Be	20	0.086	0.113	0.042	0.083	0.105	0.037
	O	76	0.031	0.040	0.015	0.030	0.040	0.014
MgO	Mg	60	0.092	0.094	0.039	0.107	0.100	0.033
	O	53	0.098	0.102	0.042	0.113	0.103	0.034
Al_2O_3	Al	17	0.275	0.442	0.198	0.320	0.287	0.110
	O	76	0.100	0.161	0.072	0.115	0.076	0.029
	Al	20	0.245	0.395	0.177	0.286	0.260	0.095
	O	65	0.117	0.189	0.085	0.135	0.094	0.034
$MgAl_2O_4$	Mg	30	0.059	0.087	0.038	0.069	0.044	0.017
	Al	30	0.117	0.173	0.077	0.137	0.112	0.043
	O	59	0.116	0.171	0.076	0.134	0.079	0.028
SiC	Si	93	0.028	0.031	0.013	0.031	0.056	0.018
	C	16.3	0.107	0.119	0.050	0.117	0.205	0.067
AlN	Al	50	0.071	0.070	0.030	0.088	0.120	0.043
	N	50	0.066	0.066	0.028	0.080	0.090	0.033

volume. According to the first definition, the damage rates p_1 and p_2 for each component would be

$$p_1 = \frac{D_1}{N_1}; \qquad p_2 = \frac{D_2}{N_2}.$$

When divided by the total flux of the projectiles, these values are equal to the damage cross-sections shown in Eq. (6), which are independent of the atomic densities of the components. The second definition leads to

$$\mathrm{DPA} = \mathrm{DPA}_1 + \mathrm{DPA}_2 = \frac{D_1}{N_1 + N_2} + \frac{D_2}{N_1 + N_2} \qquad (7)$$

and would have the advantage of the total damage DPA being simply written as the sum of the two additives DPA_1 and DPA_2. From a physical point of view, DPA_1 and DPA_2 can be interpreted as displacement damage of the related target components and, for the specific case of monoatomic targets, the usual DPA definition follows.

The individual contributions of each constituent to the total damage are summarized in Tables 2 and 3 according to Eq. (7). These contributions are sensitive to the displacement threshold energy E_d of the individual constituents, which is the minimum energy required to permanently displace an atom from its lattice position at very low temperatures. The E_d-values for SiC have been taken from a molecular dynamics study of El-Azab and Ghoniem [42], while all others were taken from Pells, who summarized available data [40] several years ago. Because a variety of E_d-values has been used in the literature for the widely investigated α-Al_2O_3 (alumina), ranging from 17 to 40 eV for Al and 30 to 78 eV for O [41,40,10], the E_d-dependence of sublattice-specific damage rates has been calculated and shown in Fig. 4 for three different sets of frequently used E_d-values. Obviously large variations in the partial damage rates occur when the displacement threshold energies become significantly different from each other. In this example, the ratio $\mathrm{DPA}_{Al}/\mathrm{DPA}_O$ would drop from 3.8 to 0.8 if equal values of $E_d(O) = E_d(Al) = 40$ eV were used instead of more realistic ones. Even the total damage rate, which is a sum of two bars, is 20% lower for this set of equal E_d values. It is therefore important to note that, in contrast to recent assertions [10], neither the partial

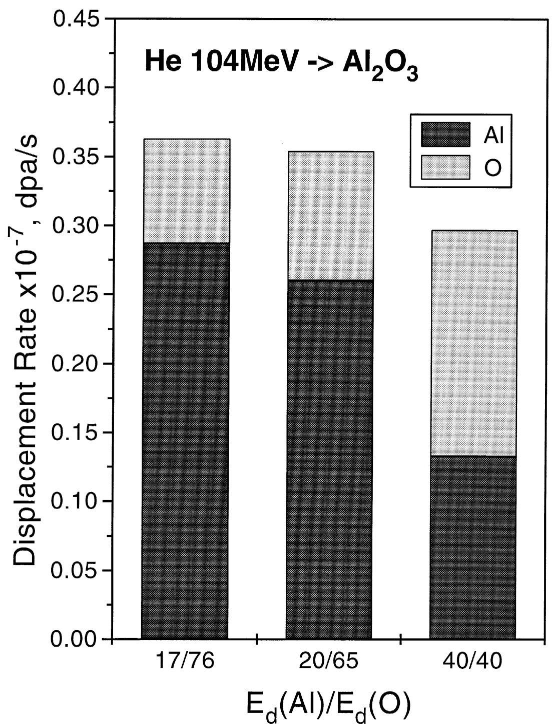

Fig. 4. Radiation damage rates in the different sublattices of Al_2O_3 bombarded by 104 MeV He^{2+} ions.

Table 3
Partial contributions to displacement damage rate (10^{-7}, dpa/s) in ceramics for several points in ITER facility. All fluxes are normalized to the total flux 10^{18} n/(m^2 s)

Material	Elem.	E_d (eV)	ITER1	ITER2	ITER3	ITER4	ITER5	ITER6
BeO	Be	20	0.083	0.093	0.088	0.063	0.040	0.074
	O	76	0.030	0.033	0.031	0.022	0.014	0.027
MgO	Mg	60	0.107	0.078	0.074	0.055	0.026	0.097
	O	53	0.113	0.086	0.080	0.059	0.029	0.103
Al_2O_3	Al	17	0.320	0.238	0.221	0.163	0.079	0.290
	O	76	0.115	0.087	0.081	0.060	0.030	0.105
	Al	20	0.286	0.212	0.197	0.145	0.070	0.259
	O	65	0.135	0.102	0.095	0.070	0.035	0.123
$MgAl_2O_4$	Mg	30	0.069	0.051	0.048	0.035	0.017	0.062
	Al	30	0.137	0.102	0.095	0.070	0.034	0.124
	O	59	0.134	0.102	0.095	0.070	0.035	0.122
SiC	Si	93	0.031	0.026	0.025	0.018	0.010	0.028
	C	16.3	0.117	0.100	0.094	0.070	0.039	0.106
AlN	Al	50	0.088	0.059	0.055	0.042	0.023	0.081
	N	50	0.080	0.055	0.052	0.040	0.023	0.073

nor the total DPA rates can be correctly described if equal E_d values are used. Especially in the case of α-alumina, a realistic description for partial DPA rates is needed to correlate various, sometimes controversial, results from different irradiation sources.

Fig. 5 presents results for displacement damage rate calculations in Al_2O_3 for several neutron environments as well as for medium energy light ion accelerators. All neutron data are normalized to one and the same flux of 10^{14} neutrons per cm^2, while the data for ions correspond to a total particle current of 1 μA per cm^2. The displacement damage in DPA units defined by Eq. (7) is additive for all sublattices of the target and can therefore be plotted for Al and O atoms as stacked bars. For the case of neutron irradiation the ratio DPA_{Al}/DPA_O of the partial displacement damage rates is about 2.8 ($E_d(O) = 76$ eV; $E_d(Al) = 17$ eV) and more or less constant for different neutron spectra. For light ion projectiles in the MeV range this ratio is about 3.8. Fig. 5 illustrates how equivalent doses for different irradiation conditions are determined. Thus, for an ITER1 first-wall position the flux of about 3×10^{14} neutrons/cm^2 would produce a total DPA rate in alumina that is equivalent to, for example, 3.5 μA/cm^2 of an 104 MeV He^{2+} ion beam. In general the light ion beams mentioned have sufficiently high ranges in ceramics to investigate bulk properties and the flexibility of the beam currents also allows the investigation of dose rate effects over several orders of magnitude.

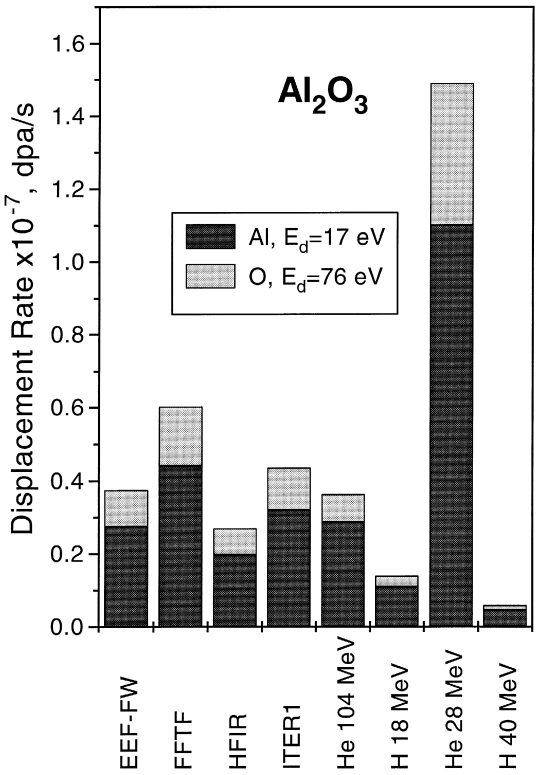

Fig. 5. Displacement damage rates in alumina for several neutron and ion sources. All neutron fluxes are normalized to the total flux of 10^{18} n/(m^2 s) and the light ions to a beam current of 10^{-2} A/m^2.

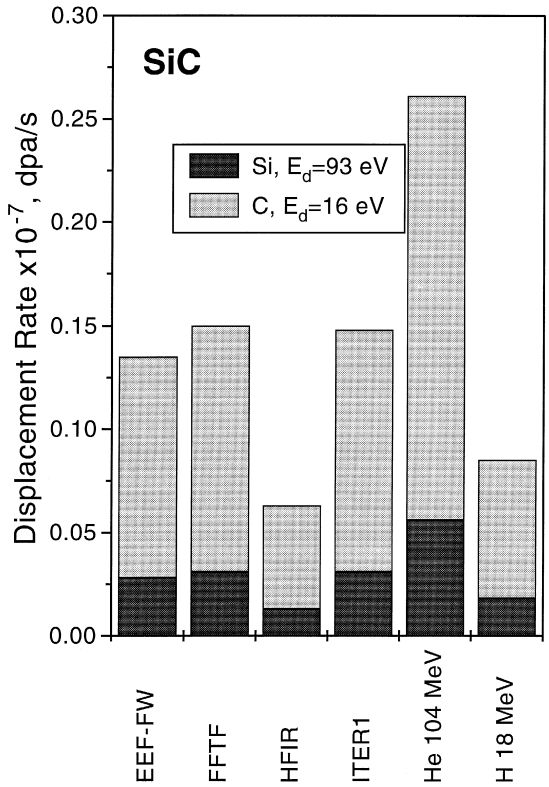

Fig. 6. Displacement damage rates in silicon carbide for several neutron and ion sources. All neutron fluxes are normalized to the total flux of 10^{18} n/(m^2 s), and the light ions to a beam current of 10^{-2} A/m^2.

Partial displacement damage rates in ceramics are presented in the Tables 2 and 3 for 104 MeV He^{2+}-ions, 18 MeV protons and several neutron environments. For magnesia–alumina spinel and β-SiC the results are plotted in Figs. 6 and 7, respectively. Our calculations show that in silicon–carbide, the defect-production rate during ion irradiation reaches values similar to neutron irradiation environments at lower ion currents than in alumina. Thus, for example, 104 MeV He^{2+} ions with a beam current of 1.7 μA/cm^2 could produce the same damage rate in SiC as that of the ITER1 spectrum. Concerning the ratios of partial damage rates for BeO, MgO and SiC, only minor differences can be found among the various irradiation sources investigated, whereas for ceramics containing Al as a constituent, those ratios can deviate up to a factor of about 1.4. This deviation can be attributed to the specific neutron-induced displacement cross-sections of $^{27}_{13}Al$ used in the NJOY-program for the calculation of the PKA spectra. It might be important to note that, because of the

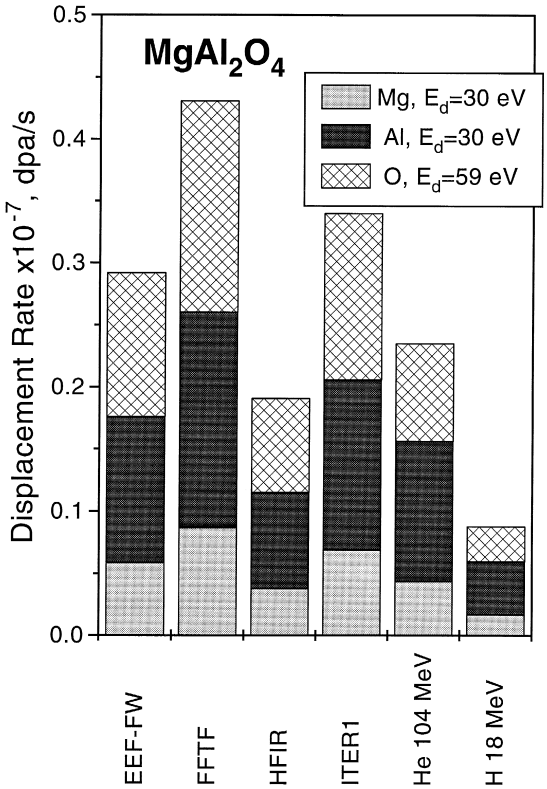

Fig. 7. Displacement damage rates in spinel for several neutron and ion sources. All neutron fluxes are normalized to the total flux of 10^{18} n/(m^2 s) and the light ions to a beam current of 10^{-2} A/m^2.

sufficiently stable ratio of the partial damage rates, both the fission neutron and light ion sources that are being investigated are well-suited to simulate fusion environments, as long as the irradiation damage is characterized in terms of DPA. The relative stability of that ratio is not obvious because it has been shown that the displacement efficiencies in various oxides [37] and the partial displacement rates in SiC [39] are subject to significant variation at low recoil energies. However, those features might be averaged by the more-or-less broad PKA spectra characteristic of the irradiation sources used.

5. Summary

We have performed displacement damage calculations for BeO, α-Al_2O_3, AlN, MgO, $MgAl_2O_4$ and SiC using a method based on the direct solution of Boltzmann transport equations for knocked-on atoms. We have compared neutron and ion irradiations using the same physical and numerical approach. We applied this method to some neutron and high-energy light ion sources that are available for qualifying ceramics for fusion reactor applications.

The results reveal that a mixed-spectrum reactor like HFIR can match specific Tokamak regions well, as shown for oxygen PKAs, although the general fusion-specific PKA spectra cannot be represented by existing higher fluence irradiation sources. This result is in agreement with existing knowledge concerning displacement damage.

The sublattice-specific displacement damage rates follow neither the stoichiometric ratios of polyatomic materials nor the ratio of the displacement threshold energies. For all neutron environments and ceramics considered here, the calculated ratios of the sublattice-specific damage rates are similar within 3% accuracy. Unless no Al atoms are present in ceramics, these ratios coincide with those for ion irradiation with 5% accuracy. The results are quite different for Al_2O_3 and $MgAl_2O_4$. In these cases the ratios of the sublattice-specific damage rates can vary by a factor of 1.4 for different irradiation environments.

The displacement damage rates obtained in this paper can be also used to renormalize the DPA dose for various irradiation experiments that have already been published.

Acknowledgements

The authors are grateful to Professor K. Ehrlich for constructive discussions. This project is supported by governmental contract No. X222.82 for Bilateral Scientific-Technological Cooperation.

References

[1] Ch. Kinoshita, S.J. Zinkle, J. Nucl. Mater. 233–237 (1996) 100.
[2] S.J. Zinkle, E.R. Pells, J. Nucl. Mater. 191–194 (1992) 58.
[3] T. Shikama, G.P. Pells, J. Nucl. Mater. 212–215 (1994) 80.
[4] C. Patuwathavithane, W.Y. Wu, R.H. Zee, J. Nucl. Mater. 225 (1995) 328.
[5] A.V. Rezvoushin, V.M. Chernov, and B.K. Kardashev, J. Nucl. Mater, in press.
[6] G.P. Pells, J. Nucl. Mater. 184 (1991) 177.
[7] G.P. Pells, B.C. Sowden, J. Nucl Mater. 223 (1995) 174.
[8] G.P. Pells, J. Nucl. Mater. 184 (1991) 183.
[9] P. Jung, Z. Zhu, H. Klein, J. Nucl. Mater. 206 (1993) 72.
[10] W. Kesternich, F. Scheuermann, S.J. Zinkle, J. Nucl. Mater. 219 (1995) 190.
[11] A. Möslang, E. Daum, R. Lindau, Proc. 18th Symp. on Fusion Technology, Elsevier, Amsterdam, 1995, p. 1313.
[12] R. Lindau, A. Möslang, J. Nucl. Mater. 233–237 (1996) 1294.
[13] R. Yamada, S.J. Zinkle, G.P. Pells, J. Nucl. Mater. 209 (1994) 191.
[14] T. Shikama, M. Narui, Y. Endo, A. Ochiai, H. Kayano, J. Nucl. Mater. 191–194 (1992) 544.
[15] R.H. Goulding, S.J. Zinkle, D.A. Rasmussen, R.E. Stoller, J. Appl. Phys. 79 (1996) 2920.
[16] A. Ibarra, R. Vila, F.A. Garner, J. Nucl. Mater. 233–237 (1996) 1336.

[17] K. Noda, T. Nakazawa, Y. Oyama, H. Maekawa, J. Kaneda, C. Kinoshita, Fusion Eng. Des. 29 (1995) 448.
[18] K. Noda, T. Nakazawa, Y. Oyama, D. Yamaki, Y. Ikeda, J. Nucl. Mater. 233–237 (1996) 1289.
[19] D.M. Parkin, C.A. Coulter, J. Nucl. Mater. 85&86 (1979) 611.
[20] J. Lindhard, V. Nielsen, M. Scharff, Dan. Vid. Selsk. Mater. Fys. Medd. 36 (1968) 1.
[21] J. Lindhard, V. Nielsen, M. Scharff, P.V. Thomsen, Dan. Vid. Selsk. Mater. Fys. Medd. 33 (10) (1963) 1.
[22] J.M. Torrens, M.T. Robinson, M.J. Norgett, Phys. Rev. B 9 (1974) 5007.
[23] L.R. Greenwood, Radiation Damage Calculations for Compound Materials, Advisory Group Meeting on Nuclear Data for Radiation Damage Assessment and Related Safety Aspects, IAEA, Vienna, Austria, Sept. 19–22, 1989.
[24] P.V. Vladimirov, Yu.D. Lizunov, Radiat. Eff. 139 (1996) 109.
[25] Y.D. Lizunov, A.I. Ryazanov, Radiat. Eff. 60 (1982) 95.
[26] Y.D. Lizunov, A.I. Ryazanov, preprint IAE-5298/11, 1991, Moscow.
[27] Y.D. Lizunov, A. Möslang, A.I. Ryazanov, J. Nucl. Mater., to be published.
[28] G.H. Kinchin, R.S. Pease, Rep. Prog. Phys. 18 (1955) 1.
[29] P.F. Rose, C.L. Dunford, US National Nuclear Data Center, Brookhaven National Laboratory, Upton, NY, 11973, Oct. 1991.
[30] R.E. MacFarlane, D.W. Muir, R.M. Boicourt, The NJOY Nuclear Data Processing System, Los Alamos National Laboratory report LA-9303-M, (ENDF-324), May 1982.
[31] G.F. Dell, A.N. Goland, J. Nucl. Mater. 102 (1981) 246.
[32] R.A. Forrest, Reference Neutron Spectra for Inventory Calculations, Harwell Laboratory, 1991.
[33] P.I.H. Cooke, R. Hancox, W.R. Spears, Reference Tokamak Reactor, Culham Report CUL-R 298, 1990.
[34] E.P. Lippincott, D.L. Oberg, Proc. Advisory Group Meeting on Nuclear Data for Radiation Damage Assessment and Related Safety Aspects, IAEA-TECDOC-263, IAEA Vienna, Austria, 12–16 Oct. 1981.
[35] P. Agnew, Nucl. Instrum. Methods B 65 (1992) 305.
[36] S.J. Zinkle, Proc. Mater. Res. Soc. Symp. 439 (1997) 667.
[37] D.M. Parkin, C.A. Coulter, J. Nucl. Mater. 101 (1981) 261.
[38] D.M. Parkin, C.A. Coulter, J. Nucl. Mater. 117 (1983) 304.
[39] W.J. Weber, R.E. Williford, K.E. Sickafus, J. Nucl. Mater. 244 (1997) 205.
[40] G.P. Pells, J. Nucl. Mater. 156&157 (17) (1988) 67.
[41] L.R. Greenwood, K.R. Smither, ANL/FPP/TM-197, 1985.
[42] A. El-Azab, N. Ghoniem, J. Nucl. Mater. 191–194 (1992) 1110.